EXPLOSIVES DETECTION BY PHOTOFRAGMENTATION AND NITRIC OXIDE-OZONE CHEMILUMINESCENCE: PORTABILITY CONSIDERATIONS

By

RONALD WHIDDON

A THESIS PRESENTED TO THE GRADUATE SCHOOL
OF THE UNIVERSITY OF FLORIDA IN PARTIAL FULFILLMENT
OF THE REQUIREMENTS FOR THE DEGREE OF
MASTER OF SCIENCE

UNIVERSITY OF FLORIDA

2007

To my father, who is a model of wisdom, patience and charity.

TABLE OF CONTENTS

LIST OF TABLES

LIST OF FIGURES

LIST OF ABBREVIATIONS AND SYMBOLS

CAD	computer aided drafting
CL	chemiluminescence
DNT	dinitrotoluene
HMX	high molecule weight RDX
IED	improvised explosive device
IMS	ion mobility spectrometer
LIF	laser induced fluorescence
LoD	limit of detection
NO	nitric oxide
NO_2	nitrogen dioxide
NO_2*	excited state nitrogen dioxide
NOCL	nitric oxide ozone chemiluminescence
O_3	ozone
PETN	pentaerythritol tetranitrate
RDX	royal demolition explosive
REMPI	resonance enhanced multiphoton ionization
STP	standard temperature and pressure
TATP	triacetone triperoxide
TEA	themal energy analyzer
TNB	trinitrobenzene
TNT	trinitrotoluene

Roman

M	number density of air (molecules cm^{-3} $Torr^{-1}$)
hν	radiation (photons)
f_{NO}	mass flow of nitric oxide (molecules of NO/s)
k_1	excited nitrogen dioxide production rate ($cm^3 molecule^{-1} s^{-1}$)
k_2	ground state nitrogen dioxide production rate ($cm^3 molecule^{-1} s^{-1}$)
k_3	photon emission rate (s^{-1})
k_4	excited state quenching rate ($cm^3 molecule^{-1} s^{-1}$)

Greek

Φ_{CL}	photon emission (photons/s)
Φ_t	photon emission for time t (photons)
Φ_I	photon emission up to time t (photons)
φ_{CL}	chemiluminescence quantum efficiency (dimensionless)
φ_L	luminescence quantum efficiency (dimensionless)
φ_{ex}	excitation quantum efficiency (dimensionless)
ξ_i	instrument transfer function
τ_{dwell}	dwell time in reaction chamber (s)
τ_{NO}	reaction lifetime (s)

Abstract of Thesis Presented to the Graduate School
of the University of Florida in Partial Fulfillment of the
Requirements for the Degree of Master of Science

EXPLOSIVES DETECTION BY PHOTOFRAGMENTATION AND
NITRIC OXIDE-OZONE CHEMILUMINESCENCE:
PORTABILITY CONSIDERATIONS

By

Ronald Whiddon

August 2007

Chair: James Winefordner
Major: Chemistry

The recent popularity of improvised explosive devices, and the continuing threat presented by unexploded land mines pushes the detection of hidden explosives to the forefront of scientific research. For maximum utility, a detection device should be handheld, be inexpensive, respond quickly, have little interference, and detect explosives without direct contact with the explosive device. Few instruments are available that can meet most of these requirements, primarily because measuring explosives in the vapor phase demands a sensitivity of low parts per billion to parts per trillion of explosive material.

The chemiluminescent reaction between nitric oxide and ozone has been used to detect explosives by their decomposition, which produces nitric oxide. As of yet, the instrumentation has not been scaled down to the point that it could be assembled as a handheld detector. This research is the design of a nitric oxide-ozone chemiluminescent reaction chamber that is small enough to be handheld, while still being able to detect explosives in the vapor phase. A 24 mL reaction chamber was designed that was capable of detecting mid parts per billion levels of nitric oxide, and high picogram amounts of TNT. Response times for the instrument were less than 10 s.

CHAPTER 1
EXPLOSIVES: HISTORY, CLASSIFICATION, AND DETECTION

Historical Background

Origins

Asciano Sobrero, not Alfred Nobel, is the father of high explosives. In 1846, while employed at the Turin School of Mechanics and Applied Chemistry, Sobrero discovered a method of nitrifying glycerin in a solution of nitric and sulfuric acids, which produced nitroglycerin, the first high explosive[1]. Laboratory accidents quickly convinced Sobrero that nitroglycerin was far too unstable a compound to work with. Only then did Immanuel Nobel, Alfred's father, invent a method to produce large amounts of nitroglycerin with a modicum of safety[2].

Nitroglycerin like many high explosives does not explode when exposed to flame, but it is susceptible to ignition through shock. While the compound would burn in a controlled manner, attempting to initiate detonation was extremely dangerous. In 1864 Alfred Nobel invented the blasting cap which would ignite high explosives in a controlled manner, greatly increasing the safety of explosive use.

While the problem of ignition was solved, the shock sensitivity of nitroglycerin made its transport dangerous. Alfred Nobel and his employees discovered that mixing three parts nitroglycerin with one part clay reduced this sensitivity, and in 1867 Guhr Dynamite was born. Eight years later Nobel replaced the clay with nitrocellulose, an explosive in its own right, and invented shock stable blasting gelatin, or what is now commonly known as dynamite.

All told, Nobel amassed a fortune through the production of blasting materials, but a large cost. The accidents in his factories claimed the lives of many employees, as well as his own

brother. That, added to the devastation wrought by the Nobel family product, drove Alfred to establish the Nobel peace prize[3].

The discovery of nitroglycerin in 1846 opened the floodgate of invention for high explosives. 1849 saw the emergence of ammonium nitrate, the most highly produced and abundantly used explosive material[4]; 1863 the invention of TNT, arguably the most famous high explosive; PETN in 1894; RDX in 1899. The next major addition to the high explosives arsenal did not occur until 1943 when HMX was invented.

Application

The first use of explosives for combat was recorded by Marcus Graecus, who in 700 A.D.[1] described rockets used in battle to disorient and demoralize the enemy. The introduction of the low explosive black powder to Europe in the 13th century by Friar Roger Bacon, and its subsequent perfection by Schwartz in 1320[2] quickly changed the nature of war. Heavily fortified walls that had offered good defense since the dawn of civilization proved useless against explosive breaching charges. In reality, modern combat is only an updated application of explosives.

Perhaps the most terrifying aspect of explosives is the collateral damage they effect when hidden. Anti personnel land mines, the production of which is now outlawed by a United Nations agreement, still represent a lingering threat to civilians in war ravaged areas. Improvised explosive devices (IEDs) can be extremely devastating. These devices are military ordnance such as explosive mortars, anti-vehicle mines, even bombs; modified with makeshift fuses for use as booby traps. It is in the interest of humanitarian organizations and the military to develop methods of detecting these explosive hazards.

Classification

There are several methods of classifying explosives. Each in some way relates to a physical or chemical property of the material, and each has usefulness depending on the field of application.

Rate

A first level delineation is by rate of reaction. Low explosives, such as black powder, deflagrate, meaning they burn at a fast rate. This rapid combustion produces a pressure front which propagates more slowly than the speed of sound[5]. Materials that detonate are termed high explosives. Their high rate of reaction creates a pressure front which expands faster than the speed of sound, though many can be burned without inducing detonation.

Ignition

High explosives can be further categorized by the stability of the compound. Primary explosives are those which are unstable in presence of heat or mechanical shock. They don't deflagrate. Common examples of primary explosives are mercury fulminate, lead azide, or potassium permanganate. Secondary explosives are those that are both thermally and mechanically stable. The majority of high explosives fall into this category. These explosives will deflagrate if ignited, but need the energy of primary explosion to set off a detonation[2]. Most functional explosive devices require a primary explosive linked to a secondary explosive.

Functional Group

An explosion is effectively a rapid oxidation reaction, and so explosives need both fuel for combustion and an oxidizing agent. High explosive mixtures, such as ammonium nitrate-fuel oil, separate these components, whereas molecular high explosives contain both a fuel and an oxidizer bonded together. It is common practice to classify molecular explosives by their oxidizing agent. This approach splits explosives into six categories: nitro compounds, nitrate

esters, nitramines, nitrate and chlorate and perchlorate salts, azides, and everything else[2] (Table 1-1).

Table 1-1. Explosive Classes, Examples, and Bond Structure

Nitro	Nitrate Ester	Nitramine	*orates	Azides	Other
TNT, DNT, TNB	Nitrocellu-lose, Nitroglycerin	RDX, HMX, RD-20	$KCLO_3$, $KMnO_4$	Lead Azide	TATP
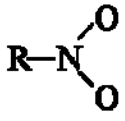	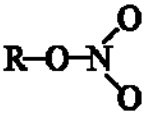	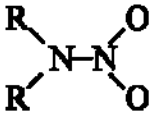	Evident from Formula	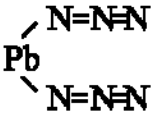	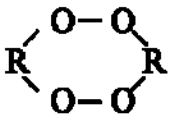

Detection of Hidden Explosives

The detection of hidden explosives is dependant on the type of explosive device being hunted. So, while there are many methods of analysis for explosive materials, few of them are suitable for detection of hidden explosives. The focus of this research is on the detection of physically implanted explosives, such as mines or IEDs. Appropriately, only field portable methods of explosives detection will be reviewed.

Three things are necessary in a hidden explosives detector: short processing time, low limit of detection, and utility. A short reaction time, less than ten seconds, minimizes the danger to the instrument operator. A low limit of detection is necessary to negate the effect of concealment as most explosives have low vapor pressures. Utility is a general consideration for the instrument operator. To be useful as a detector, the instrument should be easily carried, simple to operate, have a long duty cycle, and be accurate. A comparison of current portable detection techniques is shown in table 1-2

Table 1-2. Quick Reference of Explosives Detection Methods.

	Canine	IMS	LIF	REMPI	CL
Cost	~$50,000	$40,000	†	†	$29,000
Vapor Sampling	Yes	Yes*	Yes*	Yes*	Yes
Limit of Detection	Very Low	100 pg - 1ppm	10 ppm	10 ppm	ng - ppb
Examples	German Sheppard	GE-Vapor Tracer	†	†	Scintrex E 3500

*Limit of detection is not low enough for actual vapor phase detection. Samples are collected and vaporized at elevated temperature. CL LoD is higher because of detection at room temperature.
†Portable Instrument not available.

Canine Detection

The most successful and widely used method of detecting explosives has always been bomb sniffing dogs[6]. Frequently used in ports of entry and military bases, and even in combat, canine teams are required to have greater than 95% accuracy in detecting hidden explosives[6,7]. From a cost standpoint a bomb dog is comparable to $50,000 instrument; however, unlike an instrument, the dog requires several years of training prior to use, boarding facilities during deployment, and care in senescence. Add the fact that dogs perform best with a dedicated handler to limited availability, and the canine detector shows obvious weakness in terms of mass deployment.

Ion Mobility Spectrometry

The superstar of field deployed explosives detectors is currently the ion mobility spectrometer (IMS). The reason for their popularity is primarily their small size and light weight. Essentially the IMS is a time of flight mass spectrometer that operates at atmospheric pressure. Because of the slower movement of ions at atmospheric pressure, the drift tubes can be short yet still allow for separation. Fully functioning IMS instruments have been constructed that displace

about ½ liter[8]. At this point most major instrument manufacturers offer some type of portable explosives detector based on IMS[9].

Despite their warm reception, IMS detectors have a few characteristics that limit their effectiveness as field deployable instruments. Ionization is most often caused by radioactive nickel, a non-selective ionization source. Overabundance of ionizable molecules can flood the drift tube giving false positives. High humidity and low temperature decrease signal by forming water-analyte clusters and condensing explosive on the IMS inlet filter[1]. Additionally, the limit of detection for IMS is not very good[9]. In order to detect explosives, the sample must be concentrated by collecting on a fabric swipe. The fabric swipe is then heated in a closed sampling chamber to release vapors into the IMS.

Fluorescence

Fluorescence from explosives and explosive vapors is an area of research that has seen much interest recently. The truly seductive aspect of a fluorescence based explosives detector is that it would allow remote sensing of an explosive, a feature that is impossible in competing detection systems. While the fluorescence signal for TNT is indistinct[10], the attached nitro groups can be can be detected in that manner. Ultraviolet radiation clips the nitro groups off the parent molecule, yielding nitric oxide (NO) and nitrogen dioxide (NO_2). The NO absorbs a photon of 226 nm and is elevated to an electronically excited state. Relaxation from that state results in emission in the 226-250 nm range depending on the final vibrational level.

The major setback in LIF detection of explosives is the poor limit of detection, 10 ppm TNT at STP, well above the vapor phase concentration of TNT at room temperature[11]. To lower the limit of detection it is necessary to put the sample under vacuum, or raise the sample temperature, making this far from a standoff detection technique.

Resonance Enhanced Multiphoton Ionization

Resonance enhanced multiphoton ionization (REMPI) is similar to laser induced fluorescence in how signal is generated[12]. Once the nitro group is clipped off the parent molecule by the absorbance of a UV photon, two more photons interact with the NO molecule. The first raises NO from ground to an electronically excited state, and the second from the electronically excited state to the ionization continuum. Signal is measured with a mass spectrometer, or more simply by a pair of electrodes near the laser focus; either method makes this a non standoff technique. While detection with the mass spectrometer can detect vapor phase concentrations, it demands a non hand portable instrument. At present ion current detectors do not reach a detection limit necessary for gas phase measurement[13].

Chemiluminescence

Two chemiluminescent (CL) reactions are currently used to detect explosives[14]. The older technique detects relaxation of an excited state of NO_2 produced from the reaction of NO and Ozone (O_3). The newer CL technique measures emission from oxidation of luminol by NO_2. Chemiluminescence detectors have earned a reputation for having wide linear response, low background, and low limits of detection[15].

The nitric oxide-ozone chemiluminescence (NOCL) detector is unable to detect explosives directly. But, as most explosive groups contain multiple nitro groups attached to an organic molecule, their detection would be possible after freeing those groups from their organic backbone. One way of accomplishing this would be vapor phase combustion of the explosive, which will produce NO: this process is usually done with a heated catalyst. On the other hand, the nitro groups can be clipped off in the same way REMPI and LIF methods accomplish it, i.e., by photofragmenting the explosives with UV light. Photofragmentation can be used directly in the vapor phase, or from a solid surface.

One limitation of CL systems is their lack of absolute specificity. For an NOCL explosives detector, interference arises from reactions of O_3 with sulfur oxide, alkenes, as well as non explosive related nitrates; although, non nitrogen emission can be excluded with band pass filters. Luminol is plagued extensively with interference from a variety of oxidants: chlorates, permanganate, iodine, peroxide, ozone, sulfur dioxide, etc[16].

Summary

The potential for damage that explosives offer encourages extensive development of any new technique or augmentation that improves their likelihood of detection. The research embodied in this paper is funded by a Department of Defense grant for vapor phase explosives detection. It is the goal of this research to investigate the miniaturization of a nitric oxide-ozone chemiluminescence detector, coupled with photofragmentation for explosives detection.

CHAPTER 2
MODELING THE NITRIC OXIDE-OZONE CHEMILUMINESCENCE REACTION FOR A 24 mL REACTION CHAMBER

Introduction

After three failed attempts at making a nitric oxide-ozone chemiluminescence (NOCL) detector, computer modeling was performed to assist in understanding the nature of the reaction. The goal was to gain a solid understanding of how the signal would fluctuate with changes in reactor pressure, NO flow rate, and O_3 flow rate.

Reaction Kinetics

Kinetics of a reaction between NO and O_3 which produced NO_2 were known as early as 1954[17], yet the step responsible for emission was largely missed. The first paper to handle the chemiluminescent pathway of NO and O_3 was published in 1964 in the Transactions of the Faraday Society[18]. Clyne, Thrush and Wayne winnowed NO-O_3 reactions down to four that had appreciable effect on photon emission.

$NO + O_3 = NO_2^* + O_2$	$k_1 = 4.26*10^{-15}$ cm^3 molecule^{-1} s^{-1}	(2-1)
$NO + O_3 = NO_2 + O_2$	$k_2 = 1.6*10^{-14}$ cm^3 molecule^{-1} s^{-1}	(2-2)
$NO_2^* = NO_2 + h\nu$	$k_3 = 1000$ s^{-1}; [20]	(2-3)
$NO_2^* + M = NO_2 + M$	$k_4 = 1.49*10^{-11}$ cm^3 molecule^{-1} s^{-1}; [21]	(2-4)

Steffenson and Stedman used the reactions and kinetics for the NOCL reaction in simplified form applicable to reactions with ozone[19]. The equation (Equation 2-5) predicts the emission from an NOCL chamber operating in the continuous flow regime by including the effect that flow, pressure, and kinetics have on the signal.

$$\Phi_{cl} = (f_{NO})\varphi_{ex}\varphi_{L}\left(1 - \exp\left(\frac{-\tau_{dwell}}{\tau_{NO}}\right)\right)\xi_i \qquad (2\text{-}5)$$

The term f_{NO} is the number of molecules of NO entering the reaction chamber per second. It is found by multiplying the flow rate for the NO sample stream, the number density of that stream, and the mole fraction of NO in the stream. The equation does not allow for a maximum signal per second Φ_{cl} greater than the number of molecules of nitric oxide flowing through the reaction chamber, since f_{NO} is the only term in the equation greater than one. In reality Φ_{cl} is far less than the number of NO molecules flowing through the reaction chamber.

First, only a portion of the NO molecules are converted to excited state nitrous oxide (NO_2*), the molecule responsible for photon emission. The term φ_{ex} is the splitting ratio for this excited state. It is a constant that represents the number of molecules reacting through the equation 2-1 pathway as opposed to the equation 2-2 pathway. The value for φ_{ex} is 21%. Next, there is signal loss from quenching, φ_L. If NO_2* collides with any other molecule, it will lose energy and be unable to emit a photon. The Steffenson – Stedman splitting ratio is the number of NO_2* molecules emitting light divided by the number being quenched. This term is pressure dependant (Equation 2-4).

While the addition of reactants will result in higher signal flux for a flow system, there is also the possibility of some signal loss by the transient nature of the reactants. In a static system the reaction goes to completion before the reaction chamber is evacuated and a new mixture introduced. In the flow system, reactants are added continuously; and, reactants are removed continuously. This pumping loss is related to the rate at which molecules flow through the reaction chamber and the time necessary for those molecules to react completely.

The term (1-exp [$-t_{dwell}/t_{NO}$]) brings into the equation the pumping loss of the reaction chamber. The period t_{dwell} is the amount of time it takes a molecule to travel from the inlet of the cell to the outlet. It is calculated by dividing the volume of the reaction chamber by the flow rate

of all inlets to the chamber. The period t_{NO} is the lifetime of NO in the reaction chamber. After several seconds, the NO has been consumed and effectively the reaction is complete. This period is mathematically defined as the inverse of the sum of reaction rates k_1 and k_2 multiplied with the mole fraction of O_3 in its stream, the number density of the O_3 stream, and the ratio of the O_3 flow to total flow.

The instrumental response function is included as ξ_i. This term is static and unique for any individual chemiluminescence instrument. The term ξ_i is a catch all for the quantum efficiency of the detector, the solid angle of detection, window losses, reflectance losses, spectral overlap of the detector and emission source, etc. It is always less than one, but can only be determined through experimentation.

Model System Parameters

The chemical kinetics program Kinetica 2003, programmed by Dr. Richardson (University of Florida, Physical Chemistry) was used to model the time dependant reaction concentrations using reactions and rates given in equations 2-1 through 2-4. Kinetic modeling for both a static signal and flow modified signal was done with a differential equation program (Polymath 6.10) used to plot the differential equations 2-6 through 2-10. The Steffenson-Stedman equation (2-5) was plotted using Excel.

$$[NO]_t = [NO]_I + (-k_1[NO][O_3] - k_2[NO][O_3])dt \quad (2\text{-}6)$$

$$[O_3]_t = [O_3]_I + (-k_1[NO][O_3] - k_2[NO][O_3])dt \quad (2\text{-}7)$$

$$[NO_2^*]_t = [NO_2^*]_I + (k_1[NO][O_3] - k_3[NO_2^*]_I - k_4[NO_2^*]_I[M])dt \quad (2\text{-}8)$$

$$[NO_2]_t = [NO_2]I + (k_2[NO][O_3] + k_3[NO_2^*]_I + k_4[NO_2^*]_I[M])dt \quad (2\text{-}9)$$

$$\Phi_t = \Phi_I + (k_3[NO_2^*])dt \quad (2\text{-}10)$$

For best applicability to the existing NOCL reactor all of the modeling was performed with concentrations, pressures, and flow rates that were possible in the laboratory. NO concentration was set as 10 ppm, O_3 concentration at 1280 ppm.

Results

The temporal evolution of reactants and products, as predicted by Kinetica 2003, is shown in Figure 2-1. The photon emission is a running tally of the number of photons produced, not the instantaneous rate of emission. The result is surprising considering that the reaction emission is supposed to be a two step process. Consistent with many two step reactions the NO_2* was expected to build up, with peak emission rates occurring after peak NO_2* production. However, the model puts the peak photon emission rate right at the time of mixing. This is supported by the rate constants for the two reactions; the rate of production for NO_2* is much slower than the relaxation rate from that state, thus the intermediate cannot aggregate.

Pressure, which is related to the total count of molecules in a volume, is known in many luminescences to have to do with the quenching of excited molecules by collision energy transfer. Equation 2-4 is the quenching step in the NOCL reaction pathway. The extent of signal loss through quenching was calculated with Polymath for several pressures from 0.01 to 100 Torr (Figure 2-2). Although each successive increase in pressure represents a tenfold increase in concentration of NO, the losses due to quenching net no increase in signal, only an increase in reaction rate. Hence, CL efficiency ($\varphi_{cl,p}$) decreases with increasing pressure. This is true only for a static system, as reaction rate takes on greater importance for flow systems. To this point, only static systems have been simulated, but to properly depict the NOCL detector, we must model under continuous flow dynamics. Plotting equation 2-5 using a reactor pressure of 1 Torr and flow rates of 100 to 1000 mL/min yields the signal response shown in figure 2-3. The results show that highest signal is found for about equal flow rates of NO and O_3. The basic difference

between this plot and the static systems results is the inclusion of a pumping loss on total signal. Excel and Polymath were used to solve the series of differential equations 2-6 through 2-10 to check the validity of the Steffenson – Stedman equation. The surface is similar in shape to figure 2-3, but has a hundredfold higher signal.

Discussion

By modeling the chemiluminescent reaction of NO with O_3, we are able to come to a greater understanding of the temporal dynamics of the reaction. The temporal dynamic shows that pressure will have a two fold effect on efficiency as increasing it will decrease pumping losses, but increase quenching loss. Finally we see that slightly higher flow rates of NO compared to O_3 flow will yield the highest signal.

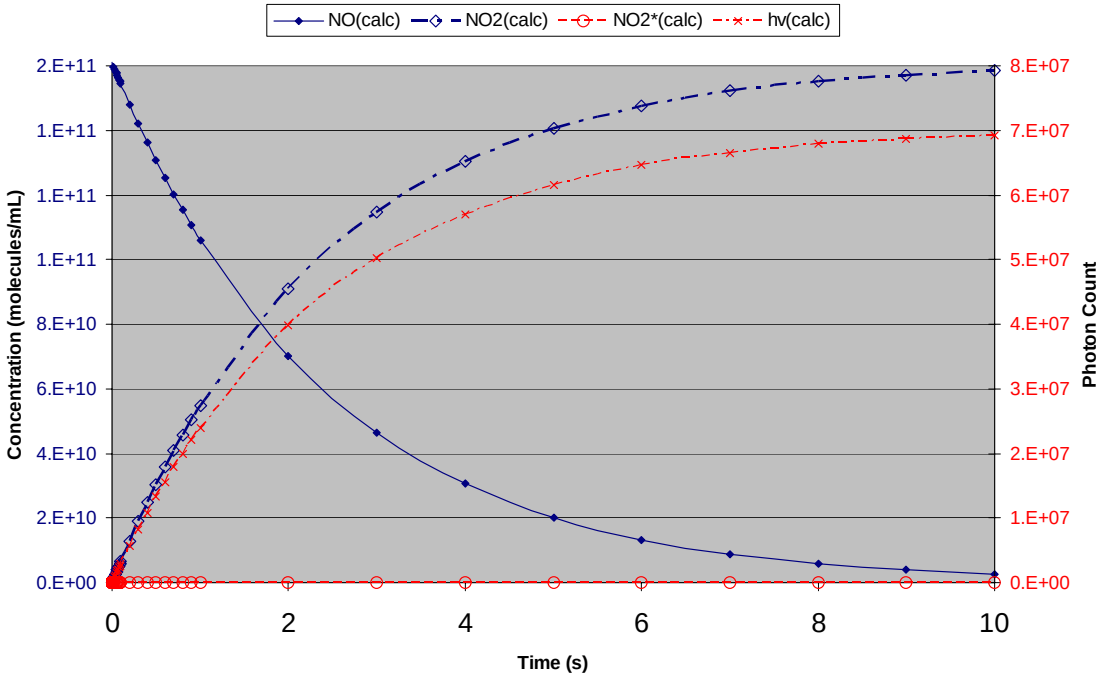

Figure 2-1: Computer Modeled NO-O_3 Reaction. The model is of a static system with no addition of reactants after time zero. Photon signal (hv) plateaus at $7*10^7$photons at 10 s.

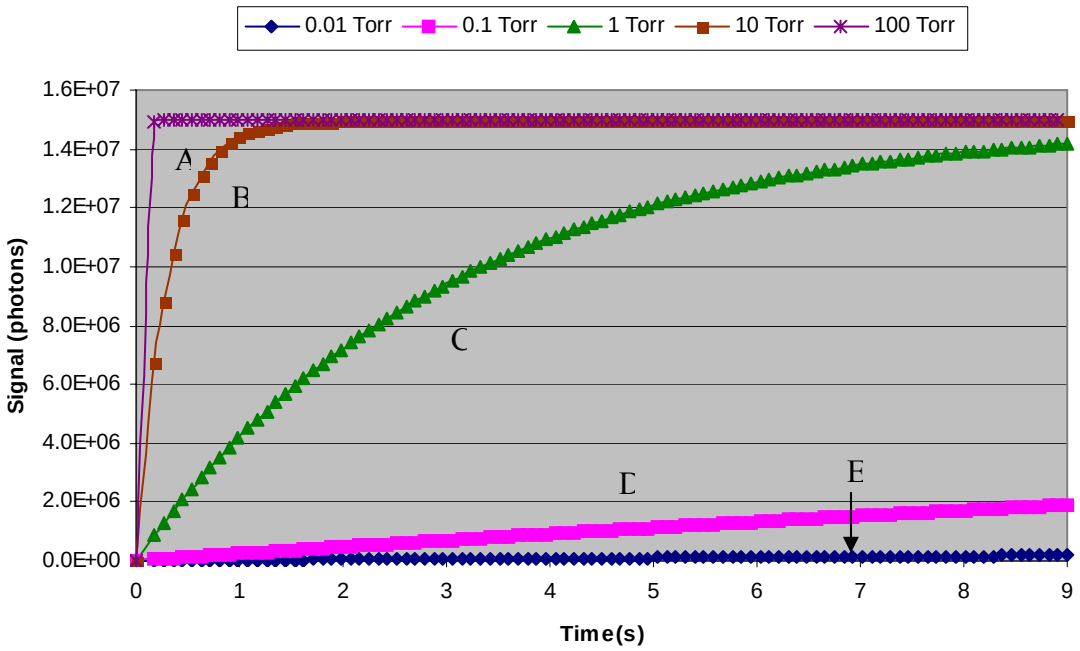

Figure 2-2: Signal Change with Chamber Pressure. Reaction chamber pressures are 0.01 Torr A, 0.1 Torr B, 1 Torr C, 10 Torr D, and 100 Torr E. All pressures reach the same emission limit of $1.5*10^7$ photons.

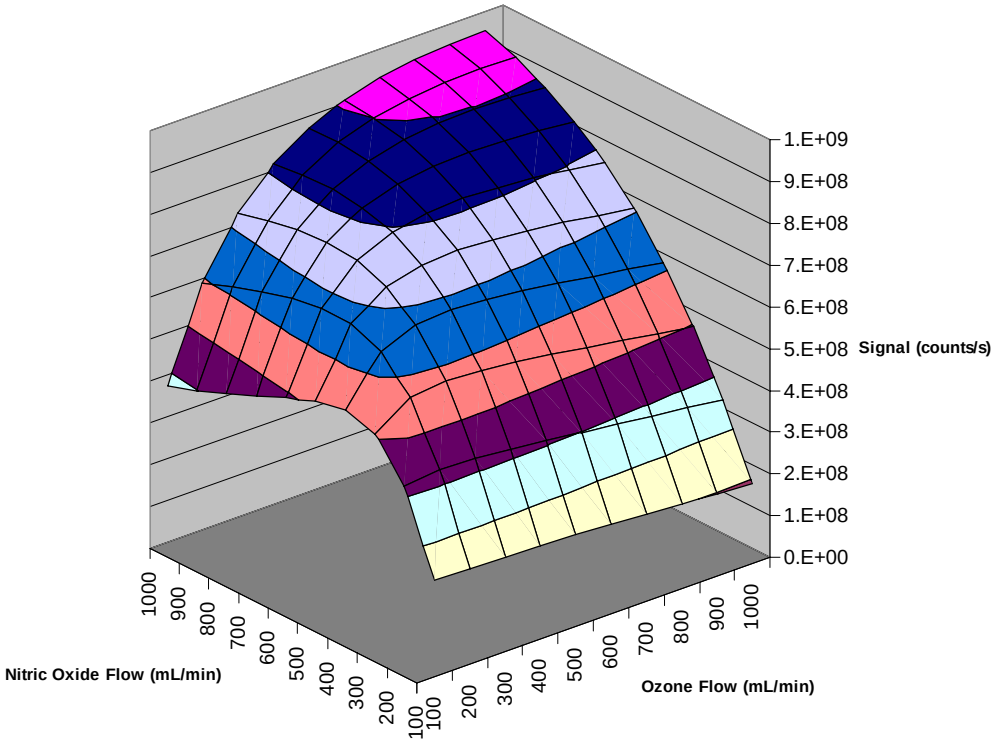

Figure 2-3: Signal Change with Reactant Flow Rate. The 3D surface plot shows that highest flow rates of NO and O_3 will give the highest signal. At the higher flow rates a plateau develops as pumping loss has a greater effect than the addition of new reagents.

CHAPTER 3
CHARACTERIZATION OF A MINIATURE NITRIC OXIDE DETECTOR: NITRIC OXIDE-OZONE CHEMILUMINESCENCE

Introduction

Nitric oxide has the distinct honor of being one of the first eight identified gases. Joseph Priestley discovered this "nitrous air" along with carbon dioxide, carbon monoxide, sulfur dioxide, oxygen, and others in his experiments published in 1776[20]. While the emission from the reaction of NO and O_3 can be seen in the night sky, as a dull reddish/brown glow, the relationship between the emission and reaction was not fully appreciated until Lord Rayleigh, in the 1920s, discovered the physical phenomenon of the emission from mixtures of NO and O_3. Kinetics of the non emissive reaction were found in the 1950s, but the full understanding of the reaction was not realized until the mid 1960s.

Background

Chemiluminescent Detectors

The end of World War II saw the proliferation of automobiles and coincidently the buildup of thick brown layers of smog in American cities[21,22]. The brown pollutant, NO_2, was traced to a byproduct of high temperature combustion, namely NO. When two molecules of NO_2 dissolve in water, nitric acid and nitrous acid are produced. (Reactions 3-1, 2, 3)These acids of nitrogen, along with sulfuric acid are responsible for acid rain devastation of the seventies and eighties[23].

This environmental danger inspired the first wave of research on NOCL detectors[24,25].

$$N_2 + O_2 \rightarrow 2NO \quad (3\text{-}1)$$
$$2NO + O_2 \rightarrow 2NO_2 \quad (3\text{-}2)$$
$$H_2O + 2NO_2 \rightarrow HNO_2 + HNO_3 \quad (3\text{-}3)$$

Nitric oxide chemiluminescence detectors have an inherent selectivity for nitrogen compounds because of their emission spectrum. They are also well suited to real time sample monitoring

since many NOCL detectors operate in the continuous flow regime. The first reported NOCL detector boasted a low ppb limit of detection; however, in order to achieve that low limit, the instrument was rather large[24]. Fontijn's reaction chamber was one liter in volume with pumping rates of 12.5 L/min. While the sensitivity of NOCL detectors was unmistakable, they were by no means portable.

A reason for such a large reaction chamber is evident from the relationship between signal, mass flow, and dwell time of the Steffenson-Stedman equation (Equation 2-5). Essentially the signal is proportional to the mass flow of NO and the reactor dwell time, so to get a large signal, use a large reactor with high flow rate. The movement away from this strategy was spurred by the desire to create instruments that could be carried by weather balloons and high flying aircraft[26-28]. This meant two things: the NOCL detector must be small and lightweight. Yet, it is impossible to reduce the volume of the reaction chamber without reducing the dwell time of the reactants. Likewise, it is impossible to reduce the pumping speed of a reaction chamber without reducing the mass flow of reactants. Both of these changes would lead to lower signal. To make up for the loss in signal brought on by miniaturization, researchers focused on ways to make the reactor more efficient.

Instrument response function is a factor for a CL detector that has nothing to do with reaction kinetics. It derives from detector amplification, optical collection efficiency, mixing dynamics etc. In miniaturizing the reaction cell, efforts were made to increase this factor. For instance, thorough reactant mixing is important in maximizing chamber efficiency[19,28]. Steffenson and Stedman found that 300 ml reaction chambers with different mixing methods gave different signals[19]. Also, chamber material was important. Coatings that were highly reflective at infra red wavelengths would also increase collection efficiency.

Ozone Generator

Ozone as an oxidizer is stronger than peroxide. It is a naturally occurring gas created by the combination of three molecules of oxygen (Equations 3-4, 3-5). The electric field in the

$$O_2 + \text{energy} \rightarrow 2\ O \quad (3\text{-}4)$$
$$2O + O_2 \rightarrow 2O_3 \quad (3\text{-}5)$$

region of an electric arc, or radiation below 200 nm can supply energy for the dissociation. The resulting radicals combine with oxygen molecules producing O_3.

One method of creating O_3 is passing oxygen in front of a mercury lamp (hollow cathode, pin, or arc) where it is photolyzed by the 185 nm line, creating a small portion of O_3. A mercury pin lamp and pure oxygen will produce 2 ppm of O_3, a level insufficient for the NOCL detector. Low levels of O_3 can be concentrated by condensing in liquid nitrogen; however, the danger of explosion is great since a steady boil off is difficult to maintain. Using high power mercury arc lamps can create higher levels of ozone, but the heat and brilliant UV light can be a safety problem.

The most efficient way to produce O_3 is with an electrical discharge. In nature, the fresh smell after a thunder storm arises from an increase in O_3 concentration produced by lightning strikes. The electric field near an electric discharge is strong enough to break oxygen and nitrogen bonds. The result is a recombination of these atoms into O_3, and excited nitrogen which gives the blue color to a spark. To reproduce this effect in an instrument, a low current high voltage is attached to an anode housed in a glass tube, inside a cathode[29]. The dielectric nature of glass prevents a true spark, so a multitude of tiny electric discharges set up between the glass and electrode. Ozone generators with 4% concentration outputs are possible when using the electrical

discharge production method. A detriment to the discharge ozone generator is the emitted RF noise.

Experimental Methods

Detector

The NOCL detector was designed and assembled in house. The reaction chamber has an interior volume of 24 mL, two thirds the volume of the next smallest reaction chamber in the literature[19]. The cavity is machined out of aluminum stock, with a 4 inch length and a 2 inch outside diameter. The inside of the chamber has a dull finish to promote a Lambertian reflection profile. The surface is not plated as aluminum already has high reflectivity in the infra red. The front of the chamber is sealed with a 1 inch low pass filter, 425nm cutoff (Edmund Optics). Mixing ports are machined in the circumference of the reaction chamber just near the front window with bores connecting to inlet tubes projecting from the back of the chamber. Figure 3-1 shows the instrument and a CAD cutaway of the reaction chamber so that the sample movement and mixing can be considered. Threads were cut in exterior front of the reaction chamber to mount in the cooled photomultiplier housing (Products for Research Inc.) creating a light tight interface between reaction chamber and detector (Figure 3-2).

The detector functions under a light vacuum of 1 Torr. It is necessary for drawing in the sample and also reduces quenching of the NO_2. A roughing pump (BOC Edwards 18) is more than sufficient for creating vacuum at total flow rates between 200 and 2000 mL/min. The pressure was adjusted with a needle valve placed between the reaction chamber and the roughing pump, and a Varian dual range pressure gauge was attached between the chamber and pump. The reaction chamber connects to the vacuum pump with ¼ inch stainless steel tubing and Cajon fittings. To minimize light leakage all tubing was either stainless steel or copper. The two inlet tubes are 1/8 inch stainless steel tubing. One tube carries the O_3 reagent gas from the ozone

generator to the reaction chamber, whilst the other carries the sample stream. Flow in each tube is controlled by mass flow controllers (Alicat Scientific) (Figure 3-3). The sample line was kept as short as possible to minimize transit time to the reaction chamber. In the final configuration, it took 2.5 s from sample introduction to signal acquisition.

Electronics

Emission is converted to an electrical signal by a 28 mm reflection mode pmt (R955, Hamamatsu Photonic). Internal gain for the R955 is $1X10^7$ and the dark count rate is on the order of tens of photons per second. To minimize the dark count rate, the pmt was placed in a cooled housing. The Peltier cooling device drops the pmt temperature to -40 ° C. At this temperature, the dark count rate was about 2-3 counts/s. The applied voltage to the photocathode was -950 V. PMT signal is recorded with a Stanford Research SR-400 fast photon counter. To isolate the photocathode events from dynode noise, the discriminator was set to trigger on the falling edge of pulses with at least -6 mV intensity. The photon counter was interfaced to the computer through a GPIB interface (USB-GPIB, National Instruments)

Sample Preparation

At this point the main goal of research was to optimize the flow and pressure settings in the newly constructed instrument. All the reactants were used in known concentrations. Ozone reagent produced by the AC-500 is factory appraised at 500 mg/L which at the onboard flow rate of 1.5 L/min translates to 2500 ppm. An NO calibration standard (spectra gases 10 ppm NO, balance N_2) was used to complete the reagent mix. In some cases, it was necessary to dilute the NO reagent. In these cases, two flow controllers were attached through a tee to the sample inlet line, one carrying the calibration standard and the other carrying house nitrogen.

Results

Since this instrument was designed and assembled in the lab, a thorough optimization regime is needed to appraise its capabilities. The two variables that need to be assessed are reaction cell pressure and reactant flow rate. Figure 3-4 shows how the instruments response varies with reaction chamber pressure. Flow rates for NO and O_3 were 600 mL/min each. The emission signal peaks at 10 Torr; however, the efficiency defined as measured signal in photons/s divided by the number of molecules of NO/s, peaks earlier at 1 Torr. So while higher signal occurs at a higher pressure, a 1 Torr reaction cell pressure will make better use of the sample. This should translate to a steeper response curve for the 10 Torr chamber and a correspondingly higher limit of detection. The drop off in efficiency from above 1 Torr is likely caused by the quenching of signal, while the drop of below 1 Torr is probably due to a too short dwell time in the reaction chamber.

A flow dependant signal surface is shown in Figure 3-5. Flow optimization was performed by measuring the signal generated for an array of flow rates of O_3 and NO that ranged from 100 to 1000 mL/min in each reagent. The measured signal (Φ_{Cl}) can be substituted into the Steffenson – Stedman equation in order to determine the instrument response function ξ_i. The first step in determining the instrument response function is converting the chemiluminescent signal, Φ_{Cl}, to the CL quantum efficiency φ_{Cl}. The term φ_{Cl} is equal to the product of φ_{ex}, φ_L, (1-exp[$-t_{dwell}/t_{NO}$]), and ξ_i.

Dividing the functions φ_{ex}, φ_L into the CL quantum efficiency reduces the signal to its (1-exp[$-t_{dwell}/t_{NO}$]) and ξ_i components. The term φ_{ex} is constant and can be directly divided out. The term φ_L is variable with the reaction chamber pressure, but since all measurements were made at 1 Torr, it is universally applied to each measurement, and thus can be removed in the same manner as φ_{ex}.

At this point the signal has been reduced to the value of (1-exp[$-t_{dwell}/t_{NO}$]) and ξ_i multiplied. When the dwell time is much greater than the reaction lifetime, (1-exp[$-t_{dwell}/t_{NO}$]) is nearly 1. The plateau seen in figure 3-6 satisfies this condition and hence is the measure of ξ_i. The instrument response factor this reactor is approximately $2.47*10^{-6}$ (dimensionless), with error of $6.3E^{-8}$. ξ_i doesn't vary with pressure, flow, or reagent concentration; so, dividing it out leaves only pumping loss. Figure 3-7 depicts the cell's pumping loss as a function of NO flow for 300 mL/min O_3 and a function of O_3 flow for 900 mL/min NO. Also included in that figure is the pumping loss predicted by the Steffenson – Stedman equation (2-5). Pumping loss appears to be proportional to a function of O_3 mass flow and the inverse to the NO mass flow, but it is not a direct relationship. It seems that the Stefenson-Stedman approximation over accounts for signal loss due to material transfer through the chamber, but this is not because of the pumping loss. The inaccuracy is caused by accounting only for emission from the molecules of NO that enter the chamber during the one second integration, and excluding emission from molecules that have been in the reaction chamber for the entire dwell time.

The final operation to be performed on this NOCL detector is the evaluation of its analytical response, and the calculation of the limit of detection. Figure 3-8 depicts the signal for the NOCL signal measured for 1 Torr of NO at concentrations from 0.50 to 10 ppm. Flow rates for NO and O_3 were each set at 600 mL/min. The experimental limit of detection, obtained under our present conditions, is approximately 300 ppb. This figure has been calculated from the conventional definition of the limit of detection, i.e., for a signal being 3 times the standards deviation of the average background signal

Discussion

A small NOCL detector was designed and constructed by our laboratory. The detector was among the smallest in existence for ozone-nitric oxide chemiluminescence. The instrument was optimized for highest efficiency by adjusting instrument flow rate and reaction cell pressure.

In the end a fair evaluation of this instrument is that it does not have the sensitivity needed for atmospheric NO monitoring. It is disappointing that the signal is so low considering that a 240 mL cell with similar mixing designed achieved pptr levels of detection[28].

Although the experimental limit of detection was found to be insufficient for the detection of explosive vapors, one should stress that this limit was obtained with a non-optimized setup. Indeed, a much lower limit is possible with optimized signal measurement. The spectral overlap between the PMT and the NOCL emission is from 600 to 900 nm. The average PMT quantum efficiency for this range is 0.041, while the emission signal represents only 6.3 percent of the total emission[30]. Multiplying the PMT quantum efficiency by the average of percent total emission from 600 to 900 nm yields a value of $6.5*10^{-4}$ (dimensionless). Dividing the measured signal by this factor gives the possible signal at 100% PMT quantum efficiency, and 100% spectral overlap, e.g. the signal measured at 0.59 ppm NO would optimally be $3.4*10^{5}$ photons/s. The noise associated with the measurement is most likely from PMT dark current, and if there were no increase in noise in the optimal system, the limit of detection would improve to 15.6 pptr. Hence, this NOCL detector could be vastly improved merely by using a better signal detection method, such as an infra red sensitive avalanche photodiode.

As previously stated, the instrument response function arises from a variety of non-reaction components that effect signal. This instrument's ξ_i of $2.47*10^{-6}$ (dimensionless) can be accounted for by estimation of some of the known efficiencies of the detector components.

The efficiency loss from the PMT, as calculated above, is $6.5*10^{-4}$(dimensionless), leaving a loss of $3.8*10^{-3}$ (dimensionless) from other sources, such as solid angle, window losses, etc.

As a result of the extensive measurements of signal at various flow rates, it is evident that the Steffenson-Stedman equation is not wholly accurate. Currently the equation only considers molecules that enter the cell during the detector integration time. The number of NO molecules should be expanded to include molecules that are in the cell for the entire dwell time, which ranges from 7.20 to 0.72 s over 200 ml/min to 2000 ml/min total flow rate.

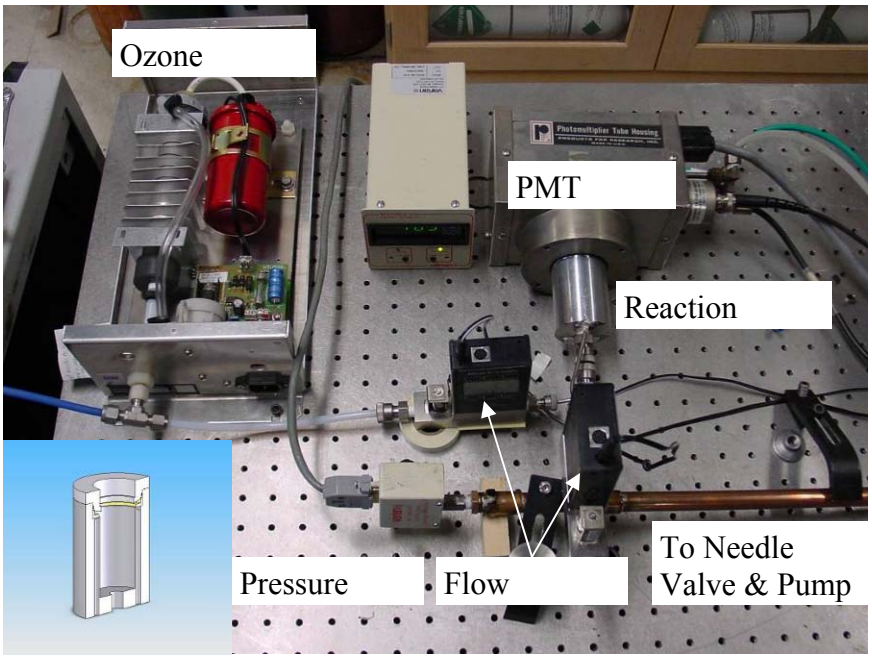

Figure 3-1: Image of NO-O_3 Instrument. Inset is cutaway of reaction chamber to highlight the circumferential mixing.

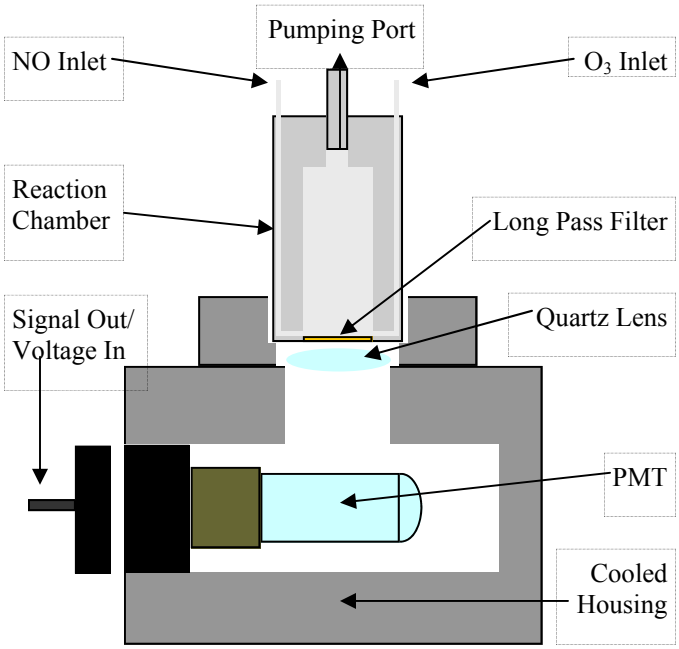

Figure 3-2: Reactor-PMT Assembly Schematic. Mixture of NO and O_3 enter the chamber near the long pass filter, and exit through the pumping port. A 1.5" focal length lens focuses light onto the PMT photocathode. Drawn to scale.

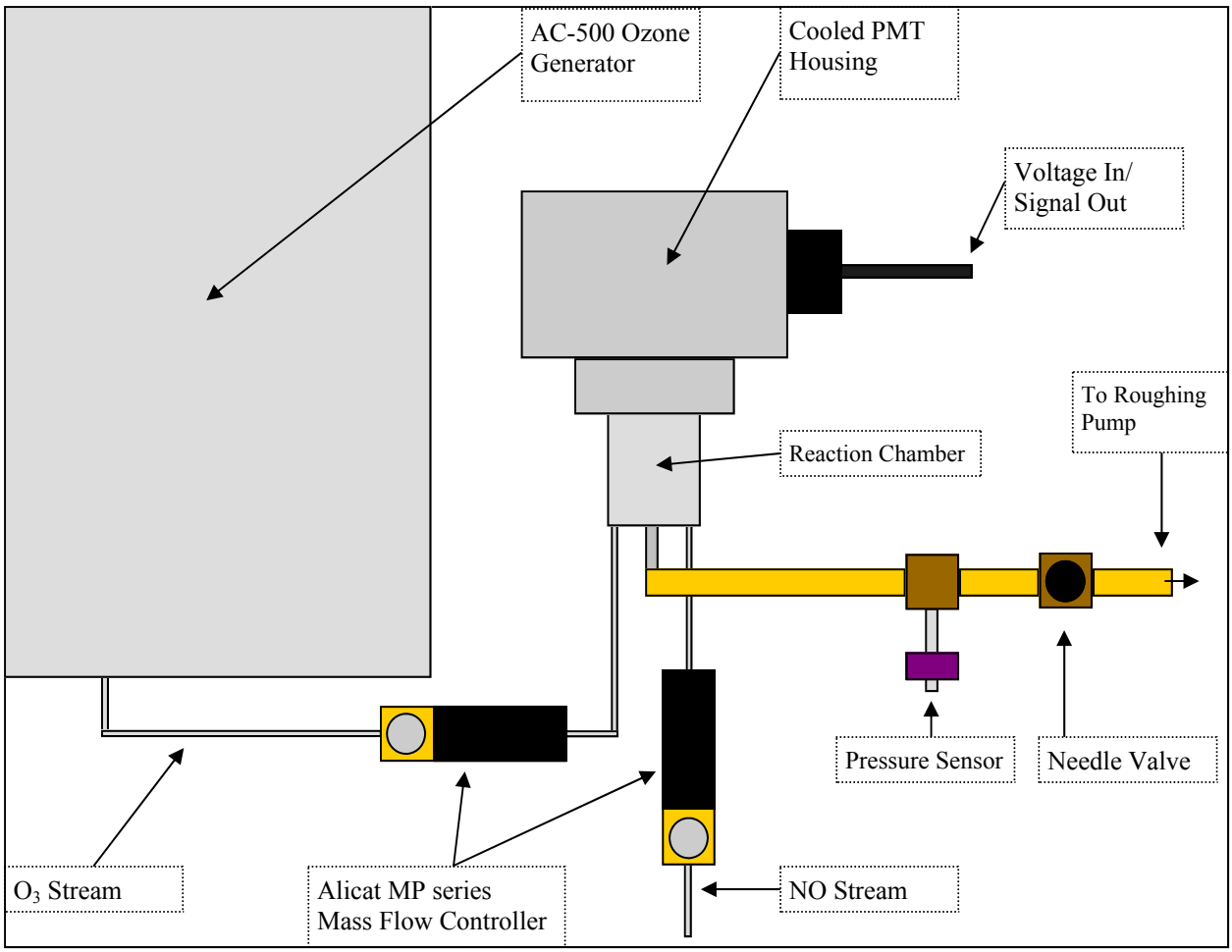

Figure 3-3: NO-O_3 Detector Schematic. Ozone from the generator and NO from a sample source flow through mass flow controllers, are mixed, and pumped out. Pressure is controlled by opening or closing the needle valve. Drawn to scale.

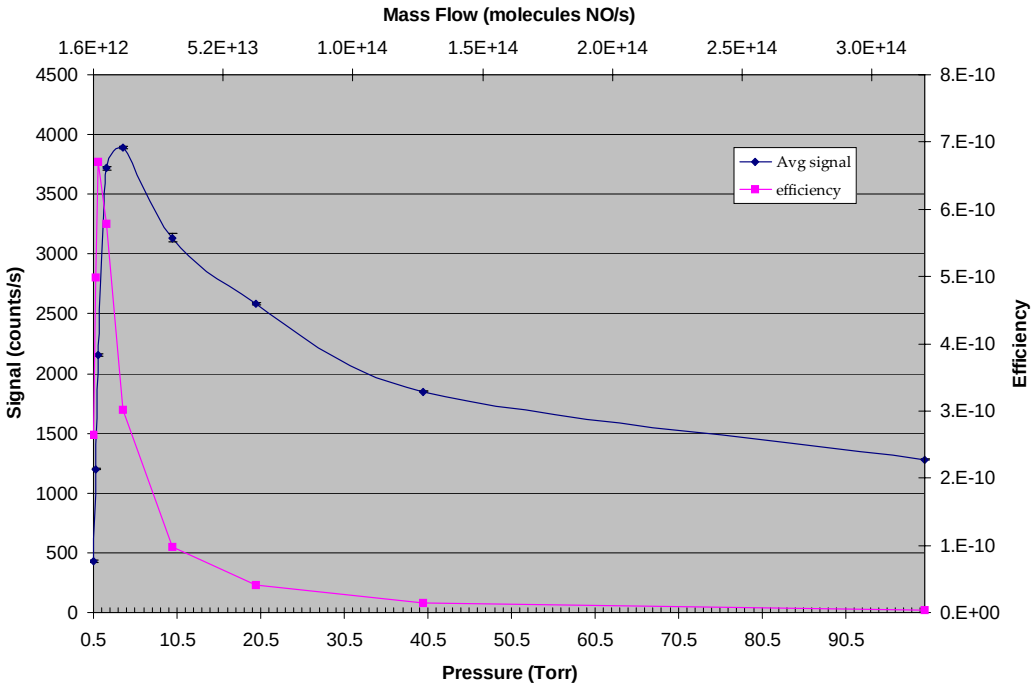

Figure 3-4: Signal as a Function of Reactor Pressure. The diamond plot is of the actual signal, while the square plot is the reaction efficiency (Photons / Molecules NO).

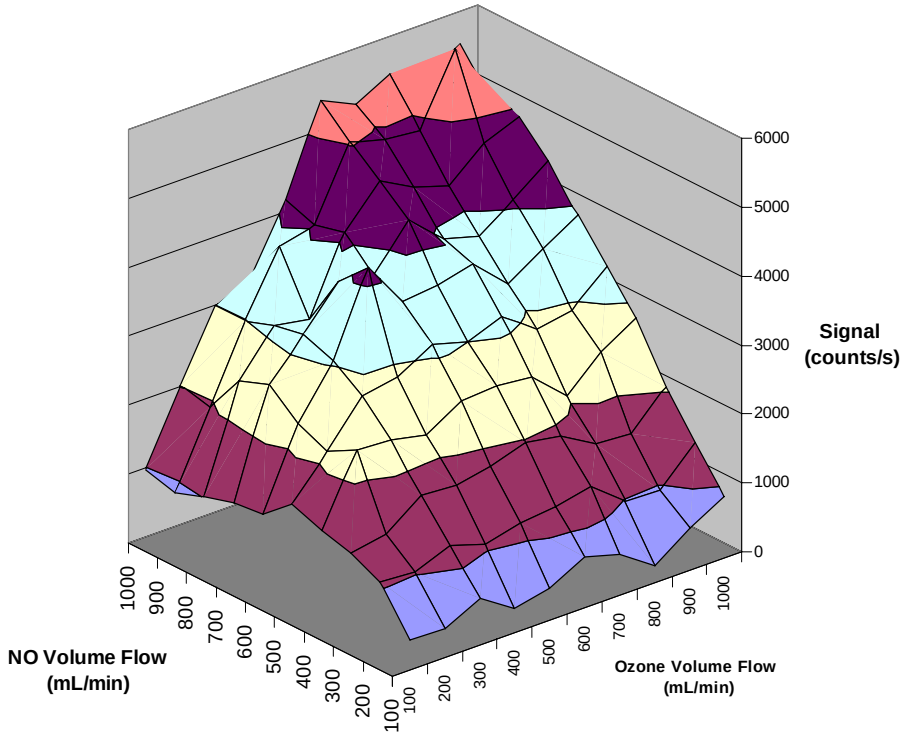

Figure 3-5: Signal as a Function of Reactant Flow Rates. 3D surface shows rapid increase in signal, but no plateau is formed as in the model result.

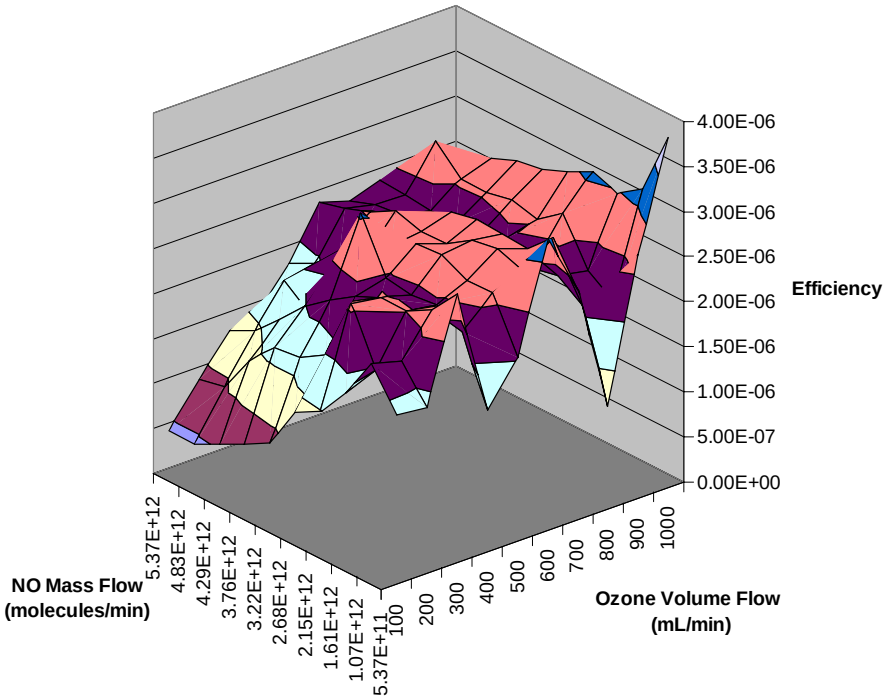

Figure 3-6: Instrument Response Function and Pumping Loss as a Function of Reactant Flow Rates. Dividing the Signal by the NO mass flow and the terms φex and φL leaves only the constant instrument response and the variable pumping loss.

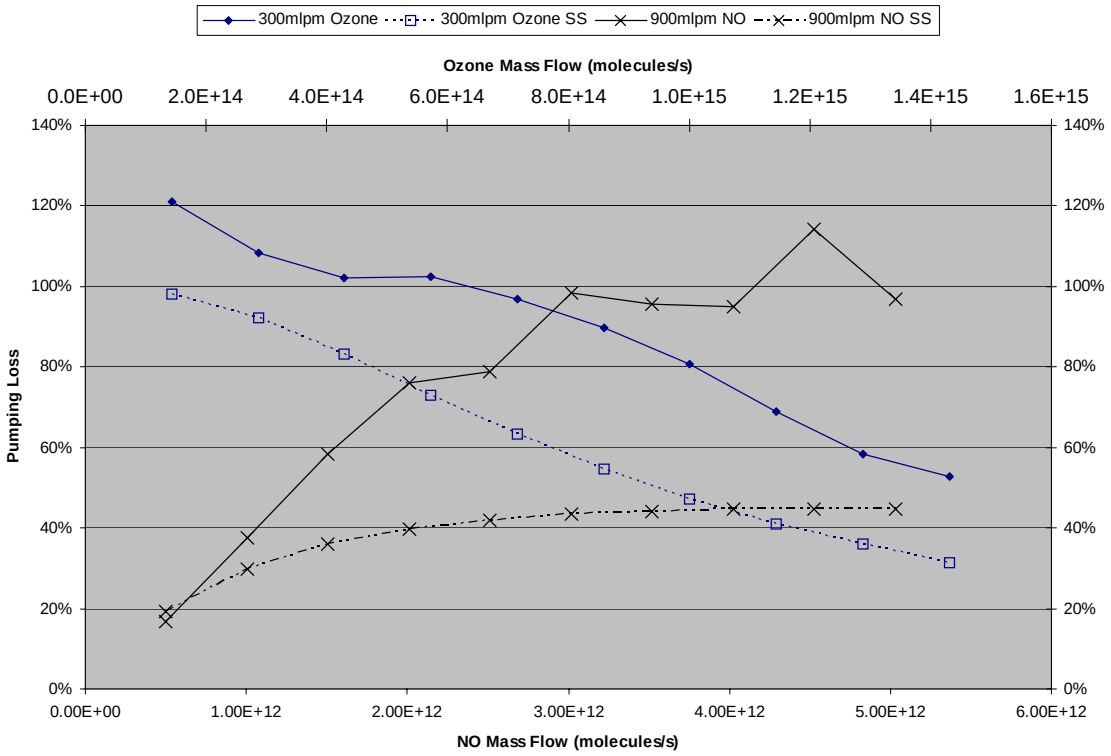

Figure 3-7: Pumping Loss from Reaction Chamber and Model. Measured pumping loss is shown in solid traces, model pumping losses in dashed lines. Negative slopes are pumping loss as a function of NO flow rate, positive slopes are Ozone flow rate dependant

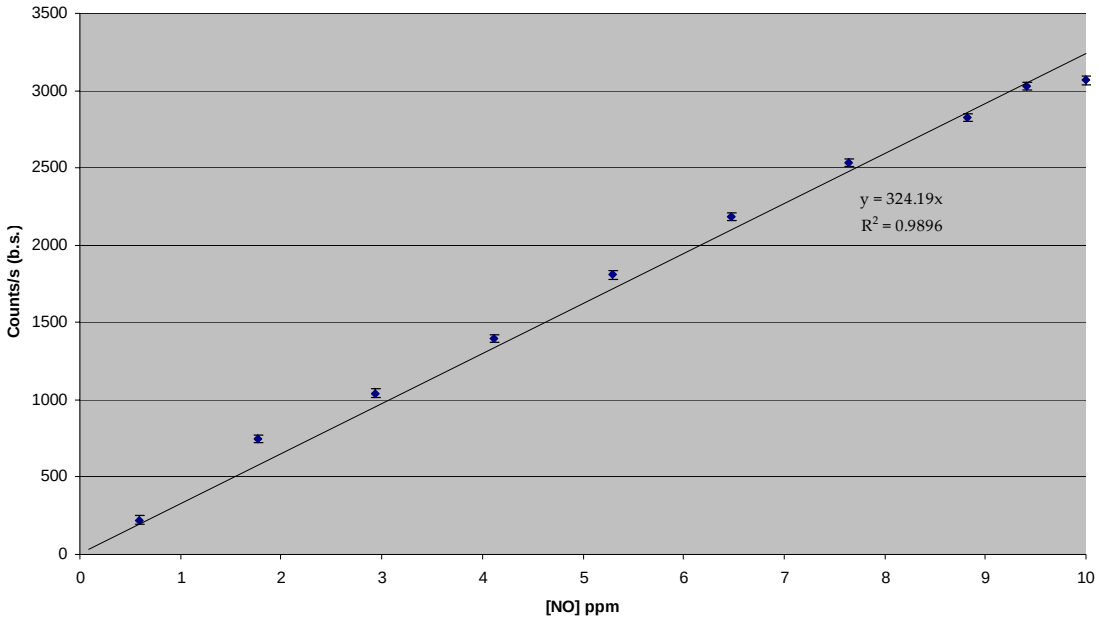

Figure 3-8: Signal as a Function of NO Concentration. The linear response of the instrument, with error bars is shown. The limit of detection is about 300 ppb NO.

CHAPTER 4
EXPLOSIVES DETECTION BY 193 nm PHOTOFRAGMENTATION WITH NOCL FRAGMENT DETECTION

Background

Material Phase and Distribution

The vapor phase concentrations for explosives are very low. Clausius-Clapeyron expressions for RDX and TNT are shown in equations 4-1 and 4-2. At 298 K, the calculated concentrations are 6.00 ppb and 9.5 ppb respectively[31]. Even with complete conversion of nitro groups to NO, the concentration is below the limit of detection for the NOCL detector studied. Sampling from a crystallized explosive effectively increases the concentration above normal vapor phase concentrations.

$$\text{Log [RDX] (pptr)} = -6473/T + 22.50 \quad (4\text{-}1)$$
$$\text{Log [TNT] (ppb)} = -5481/T + 19.37 \quad (4\text{-}2)$$

Deegan and coworkers performed extensive work on the material dispersion in droplets. Most notable is the presence of a thick ring at the edge of the deposit. As the droplet dries, evaporation happens uniformly over the surface[32]. At the edge of the droplet, the curvature means that there is a higher surface to volume ratio than at the relatively flat center of the droplet. Evaporation draws liquid to the edge, as well as suspended particles. By the time the droplet has dried, 90% of the material is contained in the outer ring[33].

Laser Photofragmentation

There are two possible laser interactions that produce nitric oxide fragments from explosive molecules. The most important is the cleavage of the nitro-carbon or nitro-amide bond on the explosive. The bond energies are about 50 kcal/mol. This bond energy equates to a photon wavelength less than 570 nm, and researches have detected fragmentation at wavelengths than

193, 227 nm, and 454 nm[31,34,35]. It is unclear whether the photolysis at 454 nm is due to a two photon process, or direct destabilization of the N-C bond. Products from cleavage are NO, NO_2, and carbon compounds.

A second laser interaction is the photolysis of NO_2. When NO_2 is impacted by a photon, this time with an energy equivalent to 250 nm the NO_2 will be excited to a semi stable state where the molecule rapidly dissociates into atomic oxygen and NO (Figure 4-1)[36-38], NO_2 has essentially the same absorption cross section as TNT and nitromethane, and is known to photolyze at the same laser wavelengths[39,40]. Maximum yield of photolysis product occurs with nanosecond laser pulses as faster pulses cause multiphoton ionization of NO_2.

Catalytic Conversion

In this instrument, the laser pulse which produces nitric oxide by photofragmentation of explosive and also photolysis of nitrogen dioxide. The photofragmentation of explosive will produce a mixture of NO and NO_2, however the production ratio is not known. It is necessary to use a second conversion technique to measure the amount of NO_2 produced by photofragmentation. Many transition metals are capable of converting NO_2 to NO when heated at 400-600 ° C. Conversion efficiencies for molybdenum, gold, and stainless steel are 100%, while platinum-gold alloy, and carbon are 57 and 95% respectively[25,41-43]. These efficiency values represent optimum values and ultimately depend on converter design

Experimental Methods

Detector

The detector used for this portion of research is the same as that used in Chapter 3. The reaction chamber is an in house design displacing 24 mL. The chamber is held at vacuum by a roughing pump. Flow rates and chamber pressure are controlled by a pair of mass flow controllers on the two inlet tubes and a manual needle valve between the chamber and pump.

The ozone reagent is produced with an EC-500 ozone generator attached through the mass flow controller to one of the chamber inlet tubes. Signal is captured by a PMT and recorded by a fast photon counter. To handle solid explosive samples a sample stage was designed and machined from aluminum (Figure 4-2). The backside of the stage has a machined surface that holds a 1 inch glass slide. The center of the recessed area has a hole covered with a quartz window to allow the laser beam to impact the sample. A small channel runs through the back of the sample stage and connects to a 1/8 inch Swagelok adapter. This channel carries air across the sample and into the reaction chamber via the mass flow controller.

A 193 nm argon fluoride excimer laser (GAM-15, GAM Inc. Orlando FL) is used to photofragment the explosive sample. The laser's pulse energy maximum is 15 mJ, the pulse length 10 ns. The laser shots were triggered externally and ranged from 0.1 to 2000 Hz. The laser was focused onto a 2 mm spot diameter on the surface of the slide by a quartz 3 inch focal length lens located between the laser and sample holder. A mechanical shutter placed between the laser and the quartz lens allowed precise control of shot number (Figure 4-3). This was necessary because the laser energy was unstable for the first twenty or so shots.

When conversion of NO_2 to NO was necessary, it was done using a stainless steel converter. An 18 inch length of $1/8^{th}$ inch diameter stainless steel tubing was bent into a coil and connected between the sample mass flow controller and the reaction chamber. The coil was heated in a sand bath to 350 ° C with a hot plate.

Sample Preparation

Samples used in this experiment were obtained from Chem Services and the office of Naval Surface Warfare Center. The samples were 2.0% mass/volume TNT in acetone and 2.5% mass to volume RDX in acetonitrile. For all experiments the volume of solution deposited was 5 *u*L. Samples were deposited on acetone rinsed 1 inch glass slides. The sample was crystallized

by solvent removal in a gentle dry nitrogen stream. The crystallized droplets were generally circular and slightly less than 1 cm in diameter. For limit of detection experiments the samples were diluted in the appropriate solvent (Acetone, 99.9%, Acetonitrile, 99.95% Fisher) prior to droplet deposition.

Results

To get an estimate of the amount of explosive ablated, it was necessary to find the general distribution of explosives in the dried droplet. Figure 4-2 inset shows the build up of a visibly raised ring on the edge of the droplet. A study of material distribution was performed to see if crystal forming explosive solution might have a different distribution compared to a suspension. This was done by measuring the NOCL signal wrought from photofragmenting explosive at positions across the dried droplet. To minimize the error from differences in size and shape of the droplet, the signal is reported in terms of the ratio of laser spot position to the radius of the droplet (Figure 4-4). It is difficult to get the amount of explosive in the droplet edge because of the poor spatial resolution the 2 mm beam diameter affords, but an estimate is shown for the droplet edge as the outer 10% of the droplet radius.

The amount of material in the droplet edge is found to be roughly 63% of the nonvolatile material. This was determined by revolving the suggested signal (Figure 4-4), which creates a disk with a raised edge. Dividing the volume of the edge by the total volume gives the percent of material in the edge. With this same method, the amount of material covered by the laser spot is found to be 0.45% of the total nonvolatile material. From the solution concentrations and volumes deposited, about 6 ng of explosive were in the laser's sample volume. The average signals collected by ablating the ~6 ng of RDX and TNT are shown in Figure 4-5. There is a large variance in the measured signal, which is caused by variations in sample crystallization.

Despite the low limit of detection this NOCL detector exhibited for nitric oxide, extremely small amounts of explosive could be measured. With the laser power at 8 mJ, a single laser pulse would produce a measurable quantity of NO from RDX, with all the material in the beam path removed by the eleventh pulse (Figure 4-6). Figure 4-7 shows the signal at various amounts of TNT; the smallest signal representing 0.5 nanograms of explosive in the beam path. Experiments with laser beam energy did not show a definite link of beam energy with signal.

It is possible that the laser beam energy is capable of photofragmenting explosive in one step of the pulse, and photolyze some of the NO_2 produced in the same pulse. This was probed by measuring the signal at three laser pump voltages with and with out the presence of a heated stainless steel converter (Figure 4-7) the data did not show an increase in the amount of nitric oxide produced, but rather the higher laser energy had a higher portion of nitrogen dioxide. It is plausible that the higher laser energies showed a higher nitrogen dioxide content because of the ablation of explosive rather than photofragmentation of NO_2.

Discussion

It was somewhat of a surprise that the detector was able to see any signal at all for explosive. However, this doesn't mean that there would be enough sensitivity to see vapor phase explosives. Even at the lowest concentration of ablated explosives there would only be 10^{12} molecules of explosive in the sample area. Atmospheric pressure would mean a sensitivity of mid parts per billion; however, the laser probe volume would have to be that entire 1 mL.

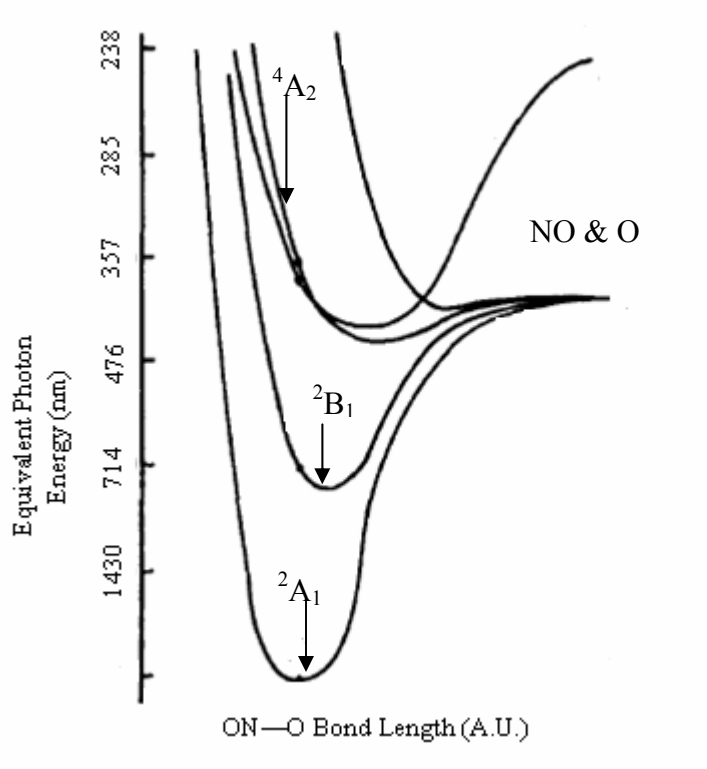

Figure 4-1: Energy Levels of NO_2 and Dissociation to NO. Excitation to the $^4A_2$ state induces dissociation of NO_2 to NO. NOCL emission arises from the $^2B_1$ to $^2A_1$ transition. Adapted from 36.

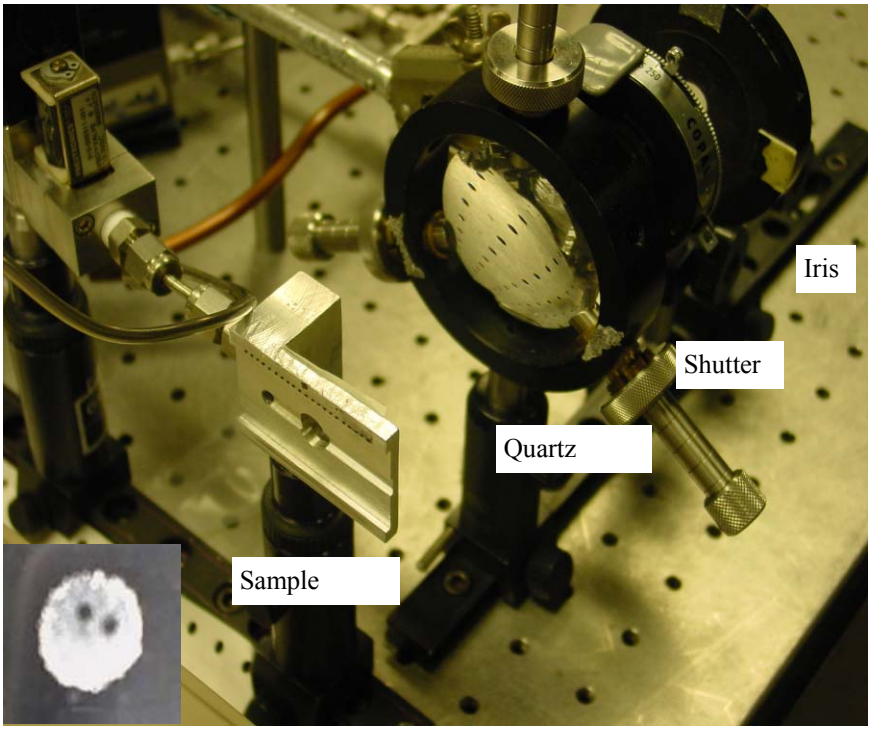

Figure 4-2: Image of Explosive Sampling Setup. Inset is of crystallized TNT on a 1 inch glass slide. The drop diameter is roughly 1 cm and two holes are laser ablation spots.

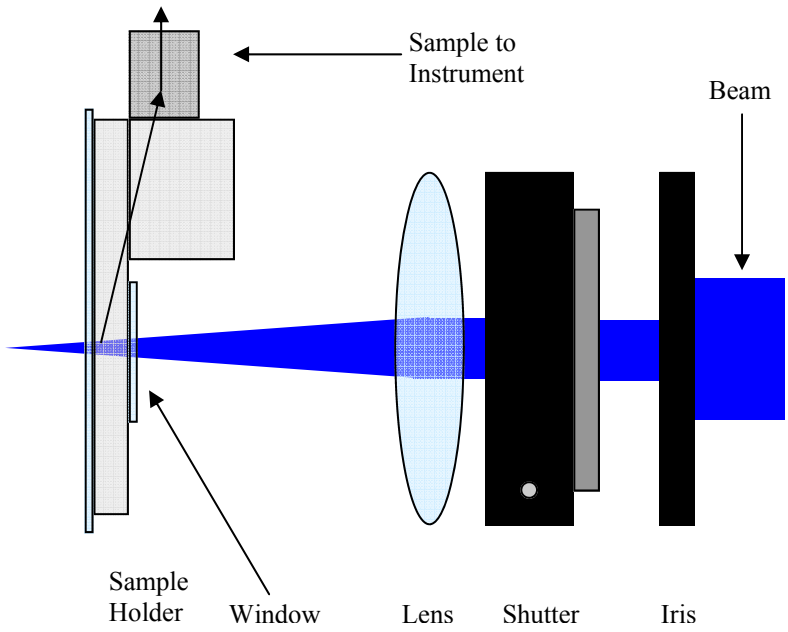

Figure 4-3: Explosive Sample Stage and Optics. Beam is trimmed to about 1/4 inch diameter by a variable iris. The mechanical shutter opens with a remote shutter cable. A 1.5 inch quartz lens focuses the beam through a quartz window onto a glass slide mounted on the backside of the sample holder. Ablated material flows into the NOCL detector (Figure 3-3).

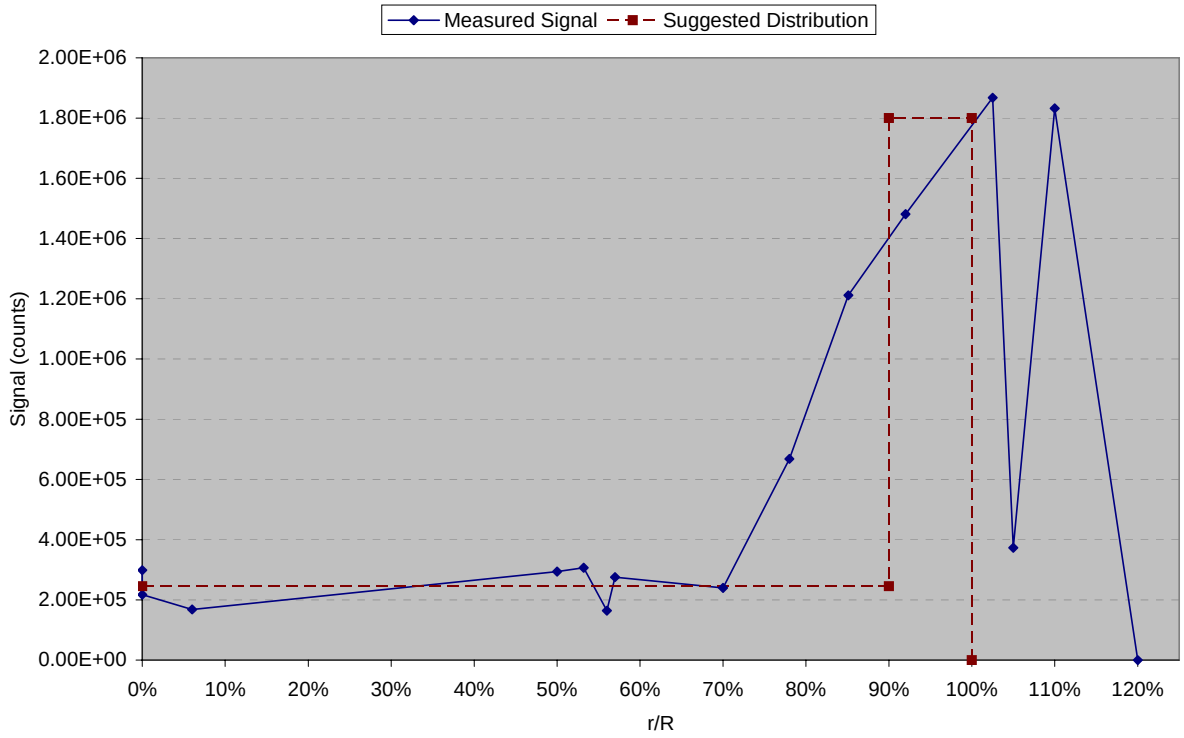

Figure 4-4: Signal from Explosive as a Function of Distance from Droplet Center. The solid line represents the measured signal from explosive droplets. The dashed line is the suggested distribution if resolution were better. R is the radius of the droplet, while r is the distance from the center of the laser spot to the center of the droplet.

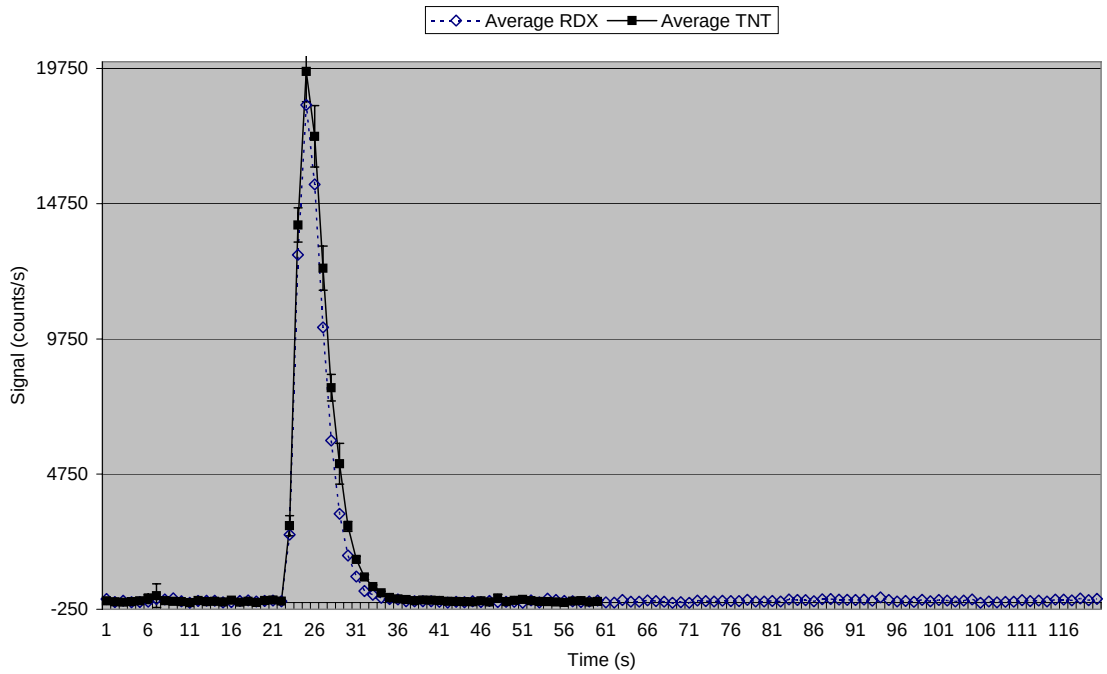

Figure 4-5: Signal Measured from Photofragmented RDX and TNT. The instrument response to both explosives is equal. Error in TNT signal is shown and very high for peak. This is partially due to very slight differences in the time axis between individual measurements.

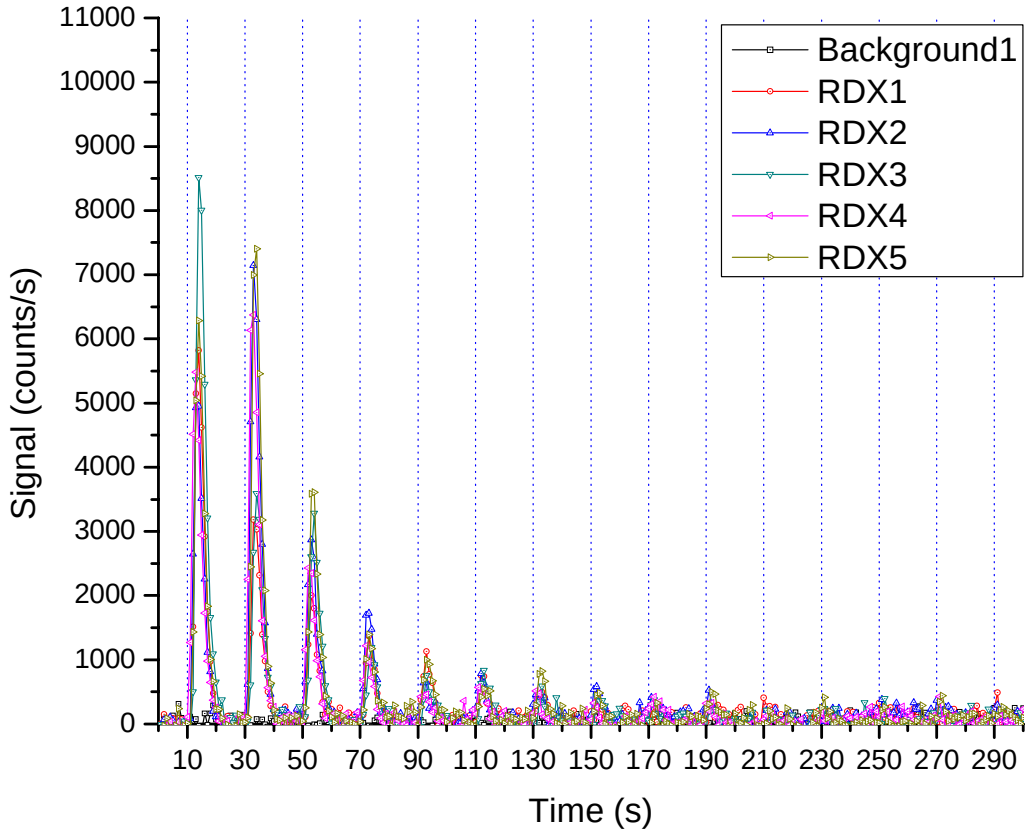

Figure 4-6: Signal Measured for Single Laser Pulses on RDX. 0.05 Hz laser rep rate was used to see if single shot detection was possible. All material in laser spot area is removed by 10 laser pulses.

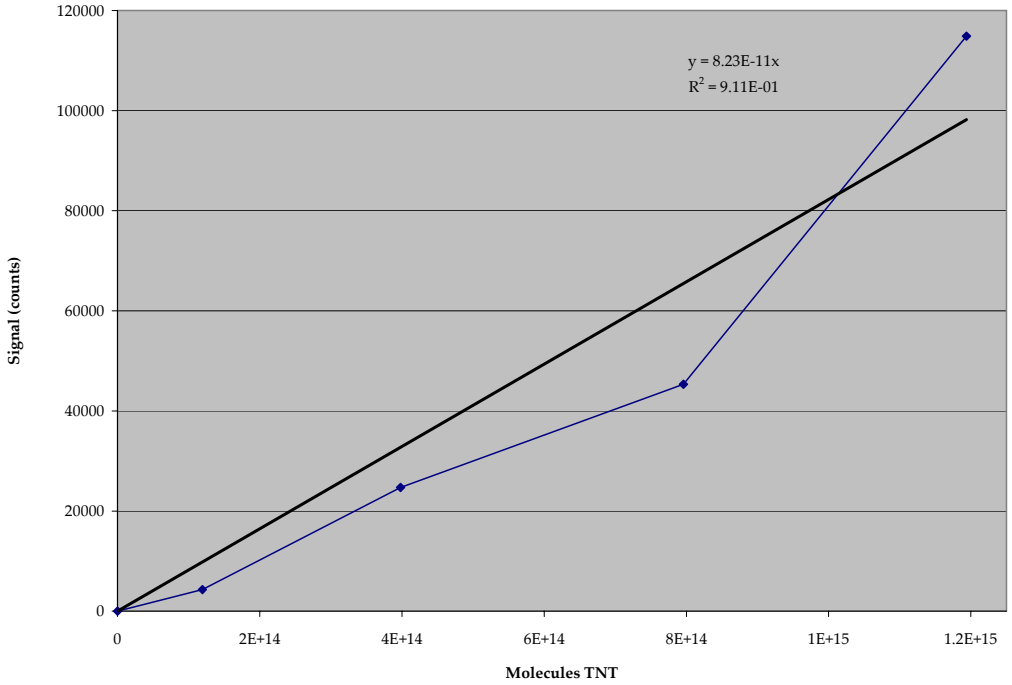

Figure 4-7: Signal Response as a Function of Photofragmentation Amount. TNT sample was diluted with Acetone to lower the total amount of crystallized explosive in the laser spot area. Straight line is linear fit with zero intercept

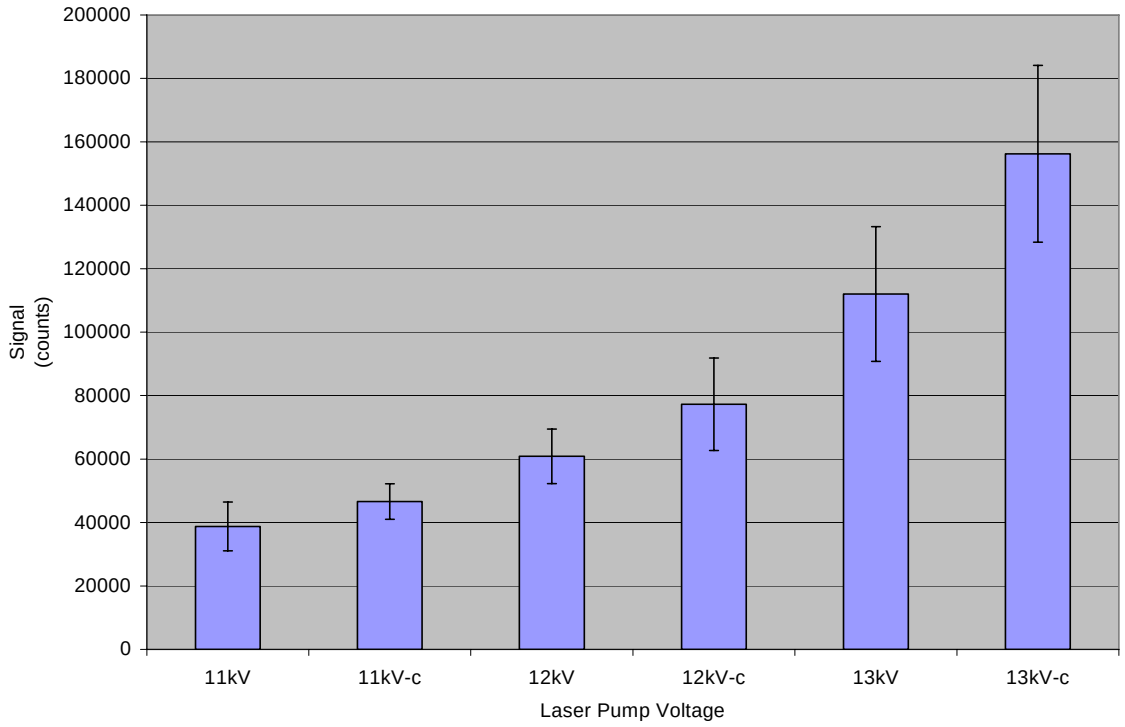

Figure 4-8: Signal as a Function of Laser Pulse Energy. Laser pulse energy was varied to observe any photolysis of NO_2 at higher laser powers. Bars with -c suffix have a stainless steel catalyst present. Higher laser powers do not indicate photolysis occurs, as the converted signal is greater in each case, indicating that at higher laser powers more NO_2 is present.

CHAPTER 5
FROM THE LAB TO THE FIELD

Summary

The original aim of research was to design a fully functioning, field portable, explosive vapor detector. And to that end, this instrument is a total failure. The limit of detection is not low enough to measure vapor phase concentrations of explosives, and frankly the detector is still too bulky for deployment

There are some simple changes that could be made to should yield better signal. The spectrum of nitric oxide lies largely in the infra red beyond the cutoff of the R955. As shown in Chapter 3, only 0.65% of the available signal can be registered because of the signal detection method. Some sources report that placing a nickel mesh in the reaction chamber shifts the emission spectrum to higher energy, moving the peak 1250 nm in the normal NOCL reaction to 800 nm in the catalyzed NOCL reaction. This would put a much larger portion of the signal in the spectral response range of the PMT[44,45]. Replacing the PMT with a large surface area avalanche photodiode, such as those offered by Advanced Photonics, would net a tenfold increase in detector quantum efficiency, as well as coverage of the entire NOCL emission spectrum. Additional physical benefits of using a photodiode would be a larger solid angle of collection by replacing the front window of the reaction chamber with the detector. And a size reduction since the thermoelectric cooling in the photodiode module is located on chip.

Even though the NOCL reaction chamber is only 24 mL, the roughing pump, cooling system, ozone generator, pmt, power supply, and especially the laser add up to an instrument that takes up four feet of bench space and weighs more than 100 lbs. Most of these components can be replaced with smaller devices without loosing sensitivity. Using a photodiode instead of the PMT would cut out the cooling apparatus, large power supply, and housing. The roughing pump

is far in excess of what is needed for the system. Tinkering in the lab yielded an ozone generator that was only a few inches long. But most important is the laser.

Laser photofragmentation is interesting, but unnecessary. Any source of high intensity ultraviolet light can photolyze NO_2 and should also be able to photofragment explosives. An emerging product that offers the monochromocity of a laser, but with a smaller size and lower energy use is the excilamp. Once developed, it could be directly substituted for the excimer laser[46]. Another photofragmentation device, developed by the NOAA laboratory, uses a 200 W mercury arc lamp focused into a quartz cell to power photolysis[47]. Otherwise it is possible to completely avoid using photofragmentation to produce nitric oxide. Catalyzed pyrolysis, as used in the TEA detector, would be a tremendous savings in both weight and energy over the excimer laser, and the mercury arc lamp. Since photofragmentation is prone to the same sources of interference as the TEA conversion, there is no loss in specificity.

LIST OF REFERENCES

1. Dolan, J., Langer, S. *Explosives in the Service of Man* (The Royal Society of Chemistry, Cambridge, UK, 1997).

2. Akhavan, J. *The Chemistry of Explosives* (The Royal Society of Chemistry, Cambridge, UK, 1998).

3. Pauli, H. E. *Alfred Nobel: Dynamite King-Architect of Peace* (L.B. Fischer, New York, 1942).

4. Fordham, S. *High Explosives and Propellants,* 2nd ed. (Pergamon Press, Oxford, 1980).

5. Dick, R. A., Fletcher, L. R., D'Andrea, V., A. Explosives and blasting procedures manual. Department of the Interior, Bureau of Mines IC 8925 Washington D.C. (1983).

6. Furton, K. G., Myers, L. J. The scientific foundation and efficacy of the use of canines as chemical detectors for explosives. *Talanta* **54**, 487-500 (2001).

7. Nambayah, M., Quickenden, T. I. A quantitative assessment of chemical techniques for detecting traces of explosives at counter-terrorist portals. *Talanta* **63,** 461-467 (2004).

8. Li, F., Wie, Z., Schmidt, H., Sielemann, S., Baumbach, J. I. Ion mobility spectrometer for online monitoring of trace compounds. *Spectrochim Acta, Part B* **57**, 1563-1574 (2002).

9. Ewing, R. G., Atkinson, D. A., Eiceman, G. A., Ewing, G. J. A critical review of ion mobility spectrometry for the detection of explosives and explosive related compounds. *Talanta* **54**, 515-529 (2001).

10. Arusi-Parpar, T., Heflinger, D., Lavi, R. Photodissociation followed by laser induced fluorescence at atmospheric pressure and 24 Celsius: a unique scheme for remote detection of explosives. *Appl. Opt.* **40**, 6677-6681 (2001).

11. Wu, D., Singh, J., Yueh, F., Monts, D. 2,4,6-Trinitrotoluene detection by laser photofragmentation laser induced fluorescence. *Appl. Opt.* **35**, 3998-4003 (1996).

12. Clark, A., Ledingham, K., Marshall, A., Sander, J., Singhal, R. Attomole Detection of Nitroaromatic Vapours Using Resonance Enhanced Multiphoton Ionization Mass Spectrometry. *Analyst* **118,** 601-607 (1993).

13. Cabalo, J., Sausa, R. Trace detection of explosives with low vapor emissions by laser surface photofragmentation-fragment detection spectroscopy with an improved ionization probe. Appl. Opt. **44**, 1084-1091 (2005).

14. Baeyens, W., Garcia-Campana, A. *Chemiluminescence in Analytical Chemistry* (Marcel Dekker, New York, 2007).

15. Jiminez, A. M., Navas, M. J. Chemiluminescence detection systems for the analysis of explosives. *J. Haz. Mat.* **106A**, 1-8 (2004).

16. Isaacson, U., Wettermark, G. Chemiluminescence in Analytical Chemistry. *Anal. Chim. Acta* **68**, 339-362 (1974).

17. Johnston, H., Crosby, H. Kinetics of the fast gas phase reaction between ozone and nitric oxide. *J. Chem. Phys.* **22**, 689-692 (1954).

18. Clyne, M. A., Thrush, B. A., Wayne, R. P. Kinetics of the chemiluminescent reaction between nitric oxide and ozone. *Trans. Faraday Society* **60**, 359-370 (1964).

19. Steffenson, D., Stedman, D. Optimization of the operating parameters of chemiluminescent nitric oxide detectors. *Anal. Chem.* **46**, 1704-1709 (1974).

20. Priestley, J. Observations on different kinds of air. *Philosophical Trans.* **62**, 147-264 (1772).

21. Thomas, M. D., *et al.* Automatic apparatus for determination of nitric oxide and nitrogen dioxide in the atmosphere. *Anal. Chem.* **28**, 1810-1816 (1956).

22. Friedel, R. A. Spectrometric investigations of atmospheric pollution. *Anal. Chem.* **28**, 1806-1810 (1956).

23. Driscoll, C., *et al.* Acid rain revisited, advances in scientific understanding since the passage of the 1970 and 1990 clean air act ammendments. *Science Links Publications* **1**, 1-24 (2001).

24. Fontijn, A., Sabadell, A., Ronco, R. Homogenous chemiluminescent measurement of nitric oxide with ozone. *Anal. Chem.* **42**, 575-579 (1970).

25. Joseph, D., Spicer, C. Chemiluminescence method for atmospheric monitoring of nitric acid and nitrogen oxides. *Anal. Chem.* **50**, 1400-1403 (1978).

26. Dickerson, R., Delany, A., Wartburg, A. Further modification of a commercial NOx detector for high sensitivity. *Rev. Sci.Inst.* **55**, 1995-1998 (1984).

27. Kondo, Y., Iwata, A., Takagi, M. Balloon-borne chemiluminescent sonde for the measurement of tropospheric and stratospheric nitric oxide. *Rev. Sci.Inst.* **55**, 1328-1332 (1984).

28. Ridley, B. A., Grahek, F. A small, low flow, high sensitivity reaction vessel for NO chemiluminescence detectors. *J. Atmos. Ocean. Tech.* **7**, 307-311 (1990).

29. Stone, E., *et al.* Lightweight ozonizer for field and airborne use. *Rev. Sci. Inst.* **53**, 1903-1905 (1982).

30. Hamamatsu, R928, R955 Spec. Sheet. (1997).

31. Swayambunathan, V., Singh, G., Sausa, R. Laser photofragmentation-fragment detection and pyrolysis-laser-induced fluorescence studies on energetic materials. *Appl. Opt.* **38**, 6447-6454 (1999).

32. Deegan, R., *et al*. Capillary flow as the cause of ring stains from the dried liquid drops. *Nature* **389**, 827-829 (1997).

33. Deegan, R. Pattern formation in drying drops. *Phys. Rev. E* **61**, 475-485 (2000).

34. Simeonsson, J., Lemire, G., Sausa, R. Trace detection of nitrocompounds by ArF laser photofragmentation/ionization spectrometry. *Appl. Spectrosc.* **47**, 1907-1912 (1993).

35. Nagakura, S. Ultra-violet absorption spectra and pi-electron structures of nitromethane and the nitromethyl anion. *Mol. Phys.* **3**, 152-162 (1960).

36. Gonzalez, A., Larson, C., McMillan, D., Golden, D. Mechanism of decomposition of nitroaromatics. Laser-powered homogeneous pyrolysis of substituted nitrobenzenes. *J. Phys. Chem.* **22**, 4809-4814 (1985).

37. Hancock, G., Morrison, M. The 193 nm photolysis of NO_2: NO(v) vibrational distribution, $O(^1D)$ quantum yield and emission from vibrationally excited NO_2. *Mol. Phys.* **103**, 1727-1733 (2005).

38. Sun, F., Glass, G. P., Curl, R. F. The photolysis of NO_2 at 193 nm. *Chem. Phys. Lett.* **337**, 72-78 (2001).

39. Ledingham, K., Kosmidis, C., Georgiou, S., Couris, S., Singhal, R. A comparison of the femto-, pico-, and nano-second multiphoton ionization and dissociation processes of NO_2 at 248 and 496 nm. *Chem. Phys. Lett.* **247**, 555-563 (1995).

40. Pastel, R., Sausa, R. Spectral differentiation of trace concentrations of NO_2 from NO by laser photofragmentation with fragment ionization at 226 and 452 nm: quantitative analysis of NO-NO_2 mixtures. *Appl. Opt.* **39**, 2487-2495 (2000).

41. Winer, A. M., Peters, J. W., Smith, J. P., Pitts, J. N. Response of commercial chemiluminescent nitric oxide-nitrogen dioxide analyzers to other nitrogen-containing compounds. *Env. Sci. Tech.* **8**, 1118-1121 (1974).

42. Bollinger, M. J., Sievers, R. E., Fahey, D. W., Fehsenfeld, F. C. Conversion of nitrogen dioxide, nitric acid, and n-propyl nitrate to nitric oxide by a gold-catalyzed reduction with carbon monoxide. *Anal. Chem.* **55,** 1980-1986 (1983).

43. Matthews, R. D., Sawyer, R. F., Schefer, R. W. Interferences in chemiluminescent measurement of nitric oxide and nitrogen dioxide emissions from combustion systems. *Env. Sci. Tech.* **12**, 1092-1096 (1977).

44. Kenner, R., Ogryzlo, E. Orange chemiluminescence from NO_2. *J. Chem. Phys.* **80**, 1-6 (1984).

45. Hartek, P., Reeves, R. Formation and reactions of the excited $O_2(A^3\Sigma^+_u)$ molecules. *Discuss. Faraday Soc.* **37**, 82-86 (1964).

46. Tarasenko, V. F. Excilamps as efficient UV–VUV light sources. *Pure Appl. Chem.* **74**, 465-469 (2002).

47. Ryerson, T. B., Williams, E. J., Fehsenfeld, F. C. An efficient photolysis system for fast-response NO_2 measurement. *J. Geophys. Res.* **105**, 26447-26461 (2000).

BIOGRAPHICAL SKETCH

Ronald James Louis Whiddon was born in Mission Viejo, California. He attended Bemidji State University in Bemidji, Minnesota, graduating with a Bachelor of Science degree in biology and chemistry. In fall 2002, he enrolled in the Analytical Division of the Chemistry Department at the University of Florida. Under the direction of Professor J. D. Winefordner, he completed his graduate studies with a Master of Science in August 2007.

.